Chapter 5: Results and discussion

To understand the mosaicism occurring in HT1, the molecular mechanisms underlying the mutation reversion need to be investigated. From previous results (van Dyk, 2005, van Dyk and Pretorius, 2005:815) it seemed as if the accumulating metabolites affected the ability of cells to repair DNA damage. To evaluate the effects on DNA repair capacity and genome stability, different assays were optimised to local laboratory conditions. These assays include the modified comet assay (to measure to capacity of cells for BER and NER), relative quantification of gene expression (to determine effects on gene expression of DNA repair proteins), microsatellite analyses (to measure genome stability), and HRM and sequencing (to assess mutation accumulation). To optimise these assays, as well as gain valuable insight into the mechanisms underlying the mutation reversion, different HT1 related models and HT1 patient material were used. The HT1 related models consist of *fah*$^{-/-}$ mice samples and metabolite exposed hepatic cell cultures. Accordingly, the focus of the current chapter is on the presentation and discussion of results obtained from these assays.

5.1 DNA damage and repair

Single cell gel electrophoresis, or comet assay, is a powerful, rapid and sensitive technique for analysing and measuring DNA damage and repair *in vitro* and *in vivo* at individual cell level (Comet Assay Interest Group). This technique can be used to study factors modifying mutagenicity and carcinogenicity, and has important uses in the field of genetic toxicology and human biomonitoring (Collins, 2004:249, Dhawan, 2006).

The comet assay works on the principle that strand breakage of the super coiled duplex DNA leads to the relaxation and reduction in the size of the large DNA molecule and these strands can be stretched out by electrophoresis (Singh *et al.,* 1988:184). The denaturation and unwinding of the duplex DNA and expression of alkali labile sites as single strand breaks occur under highly alkaline conditions. Comets then form as the relaxed and broken ends of the negatively charged DNA molecule, become free to migrate towards the anode in an electric field. According to Dhawan (Dhawan, 2006) there are two principles in the formation of comets, namely:

1. DNA migration is a function of both size and the number of broken strands of the DNA.

2. Tail length increases with damage initially and then reaches a maximum that is dependent on the electrophoretic conditions, not the size of fragments.

The standard comet assay protocol (Singh *et al.,* 1988:184) was previously optimised to local laboratory conditions for use with lymphocytes and isolated primary hepatocytes (van Dyk, 2005). In the current study, this standard protocol was modified and optimised for use with cell cultures, in specific, adherent cell lines. Personal experience has taught that for use in the comet assay, it is best to harvest adherent cells such as HepG2 cells with trypsin, as this harvesting method render intact single cells. However, harvesting with trypsin might affect downstream use of the cells, especially in sensitive applications such as the comet assay. The aim was therefore to determine the optimal time needed for the cells to recuperate from the harvesting process, before subjecting the cells to the experimental procedures. To this end, HepG2 cells were harvested and given recuperation time of 1, 2, 3, and 4 h.

In figure 5-1 A it is apparent that after even 1 h of recuperation time, there is still more than 40% DNA left in the comet tails. This is reflected in the comet class distribution (figure 5-1, B).

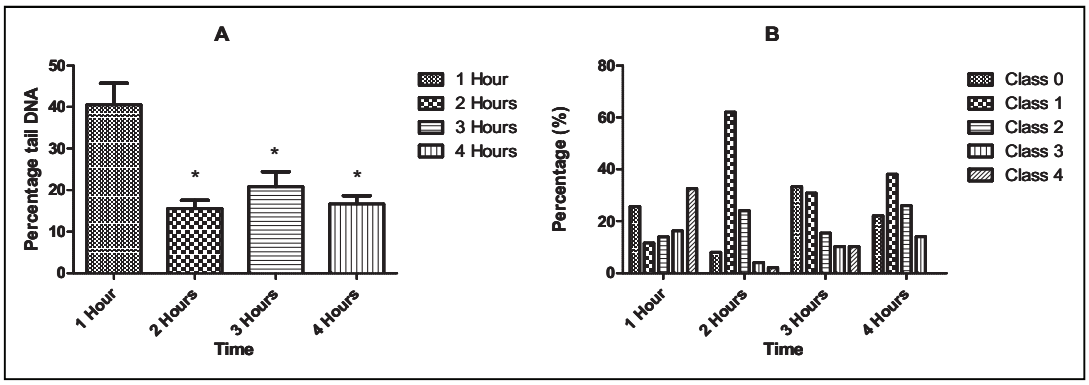

Figure 5-1. Comet assay results of recuperation time allowed after harvesting of HepG2 cells. A: Mean values of tail DNA percentages. *($p<0.05$) versus 1 hour. Error bars represent standard deviation of 50 comets scored. B: Distribution of comets in different classes.

The comet class distribution gives a representation of the ratio of comets present in each class. The comets are grouped into four classes based upon the amount of DNA present in the comet tail. Comets with less than 6% tail DNA are grouped in class 0, those with tail DNA between 6.1% and 17% in class 1, between 17.1% and 35% in class 2, between 35.1 and 60% in class 3 and higher than 60% in class 4 (Collins *et al.,* 1997:183, Singh *et al.,* 1988:184).

After 1 h of recuperation time it is apparent that more than 60% comets has a tail DNA percentage of more than 17.1%. This indicates that a high percentage of DNA damage is still present. From two hours recuperation time onwards, the tail DNA percentages (figure 5-1, A) significantly ($p<0.05$) decreases from 40% to 15% whereafter a slight increase occurs during

continuing incubation time. From these results, it therefore seems that recuperation time of two hours is enough for the cells to regain sufficient fitness for further experiments. This is supported by the comet class distribution revealing that after two hours of recuperation, the majority (70%) of comets are grouped in classes 0 and 1 (less than 17% tail DNA) with 30% of comets in classes 2, 3 and 4 (more than 17.1% tail DNA). After three hours of recuperation time, slightly less comets (64%) are present in classes 0 and 1 (less than 17% tail DNA), with 35% of comets in classes 2 to 4. At four hours recuperation time 60% of comets are grouped in classes 0 and 1 (less than 17% tail DNA) and 40% of the comets are present in classes 2 and 3 (between 35.1 and 60% tail DNA). The absence of comets in class 4 after four hours recuperation could be the result of cell death, i.e. the DNA damage in some cells might have been too extensive to repair and after four hours the cells might have died. In summary, these results indicate that the optimal recuperation time after cell harvesting is two hours, since at this point the majority of comets had less than 17% tail DNA.

A previous study by Prieto-Alamo and Laval (Prieto-Alamo and Laval, 1998:12614) illustrated that succinylacetone (SA) not only inhibits purified T4 DNA-ligase in a dose dependant manner, but also overall DNA-ligase activity *in vitro*. We, furthermore, showed that *p*-hydroxyphenylpyruvic acid (pHPPA) caused DNA damage and suggested that the metabolite impairs the DNA repair machinery (van Dyk and Pretorius, 2005:815). To further these investigations, HepG2 cells were exposed to 50 µM SA or 100 µM pHPPA for 48 h and the capacity of the cells for DNA repair was investigated with a modified comet assay. The comet assay was adapted to measure the capacity of the proteins involved in the initial steps of BER and NER to repair DNA damage (Collins *et al.,* 2001:297, Langie *et al.,* 2006:153). Results of this study were published in *Biochemical and Biophysical Research Communications* in October 2010 under the title: "Hereditary tyrosinemia type 1 metabolites impair DNA excision repair pathways." The paper is presented in chapter 6.

5.2 Gene expression profiles

The measurement of gene expression levels through mRNA levels is traditionally based on techniques such as Northern blotting, solution hybridization, and ribonuclease protection assays, or amplification of individual RNA molecules by RT-PCR with end-point product quantification (Freeman *et al.,* 1999:112, Hunt, 2010, Schmittgen *et al.,* 2000:194). However, it is now possible to quantify gene expression levels in real time. Real-time quantitative PCR is a very sensitive and flexible technique to determine levels of expressed genes (Freeman *et al.,* 1999:112, Schmittgen *et al.,* 2000:194). The use of real-time product monitoring gives improved quantification over end-point product quantification, because less sample manipulation is required, more information is obtained from each cycle, and detection during the linear range of amplification is ensured

(Freeman *et al.,* 1999:112, Schmittgen *et al.,* 2000:194). Two methods are available for the detection of DNA amplification in real-time, i.e. TaqMan® chemistry (a fluorogenic hybridization probe) and intercalating dyes such as SYBR green I (Freeman *et al.,* 1999:112). The advantage of using TaqMan® chemistry is not only that it reduces assay labour and material costs and, but more importantly, it eliminates false positives, as fluorescence can only be generated after specific hybridization of probe and target sequence.

The block of tyrosine degradation by a defective fumarylacetoacetate hydrolase enzyme results in the accumulation of upstream metabolites (Mitchell *et al.,* 2001:1777), thereby creating a sustained stress environment. To determine the effect of the stress environment on the expression of DNA repair proteins, the gene expression levels of *hOGG1* and *ERCC1* was determined in HepG2 cells exposed to the metabolites. The motivation behind the use of these genes of interest is summarised in table 5-1.

Table 5-1. Motivation for use of the specific genes of interest.

Gene of interest	Motivation
hOGG1	• Glycosylase involved in initial steps of BER (Christmann *et al.,* 2003:3) • Correlated with DNA repair capacity of BER (Hodges and Chipman, 2002:55, Lee *et al.,* 2004:9857) • Inducible (Hodges and Chipman, 2002:55, Li *et al.,* 1998:23419, Seetharam *et al.,* 2010:2531)
ERCC1	• Protein involved in the 5' incision step of NER (Christmann *et al.,* 2003:3) • Correlated with DNA repair capacity of NER (Langie *et al.,* 2007:302, Vogel *et al.,* 2000:197) • Inducible (Tsurudome *et al.,* 1999:1573)

HepG2 cells were exposed to a combination of 50 µM SA and 100 µM pHPPA for up to 96 h. RNA was extracted and cDNA synthesised with MMLV. The gene expression level of each of the genes was ascertained via quantitative Real-time PCR using TaqMan® chemistry. The expression level of the genes of interest was calculated relative to expression levels of *18S* rRNA, by way of the $\Delta\Delta C_T$ method (Livak and Schmittgen, 2001:402). The results of relative *hOGG1* expression are given in figure 5-2. Relative quantification (RQ) values of control (24 h) cells were normalised to one and the rest of the RQ values is expressed relative to control (24 h) values.

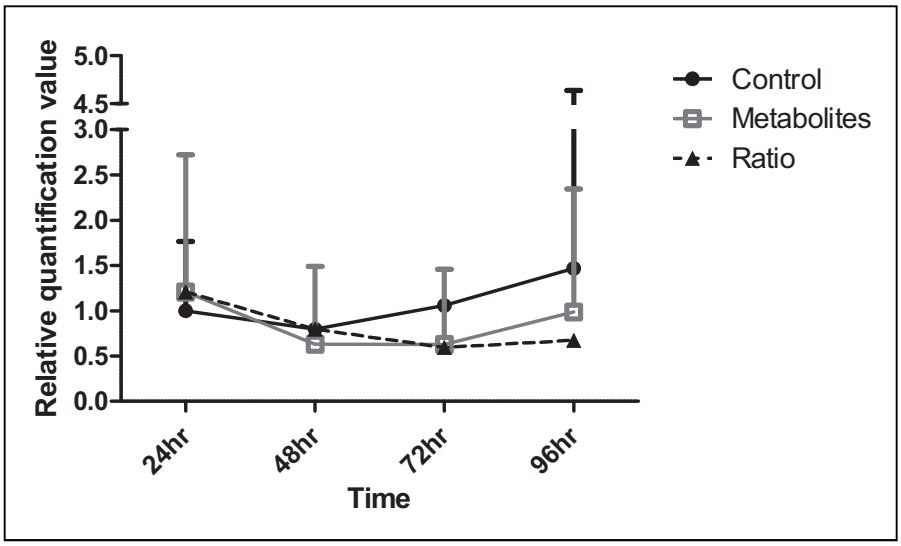

Figure 5-2. Expression of *hOGG1* by HepG2 cells after exposure to a combination of 50 µM SA and 100 µM pHPPA. The solid black line indicates relative expression of *hOGG1* in control cells; the solid grey line indicates relative *hOGG1* expression in metabolite treated cells; the dashed black line indicates the ratio between gene expression in control and metabolite treated cells. Relative quantification values are mean values for 3 biological repeat experiments done in triplicate. Error bars represent relative quantification maximum values, as calculated to 2 standard deviations of mean.

After 24 h the relative expression of *hOGG1* was 20% higher in cells exposed to the metabolite combination, compared to control cells. The expression level of the control *hOGG1* decreases with approximately 20% after 48 h. A sharper decrease of 57% is evident in cells treated with metabolites for 48 h, resulting in a 17% lower expression of *hOGG1* in metabolite treated cells compared to control cells. After 72 h the level of *hOGG1* expression in control cells increase by 25%, but the level of expression in metabolite treated cells remains almost unchanged. Up to 96 h, an almost parallel increase is evident for *hOGG1* expression levels in control and metabolite treated cells.

A two-way ANOVA, however, indicate that neither metabolite treatment nor time has a significant effect (significance: $p<0.05$) on gene expression. Also, Hanaoka and colleagues observed natural variation in *hOGG1* expression intra- and inter-individually (Hanaoka *et al.,* 2000:1255). The large standard deviation values could be a reflection of this natural variation. It would therefore seem if the observed changes in gene expression might not be significant. The observed changes (figure 5-2) might, however, be biologically relevant, as the decrease in expression after 48 h of metabolite exposure correlates with the decrease in BER repair capacity after 48 h of metabolite exposure (as measured with the comet assay (van Dyk *et al.,* 2010:32)). This also correlates with observations by other investigators that *hOGG1* mRNA expression levels reflect the cellular capacity for BER (Hodges and Chipman*,* 2002:55, Vogel *et al.,* 2002:1505). The small changes in expression levels may therefore possibly be a contributing factor (albeit small) to the observed decreased BER capacity of metabolite treated cells (van Dyk *et al.,* 2010:32).

Similar to the relative quantification of *hOGG1* expression levels, the expression levels of *ERCC1* was determined in control cells and cells exposed to a combination of SA and pHPPA. The results are shown in figure 5-3.

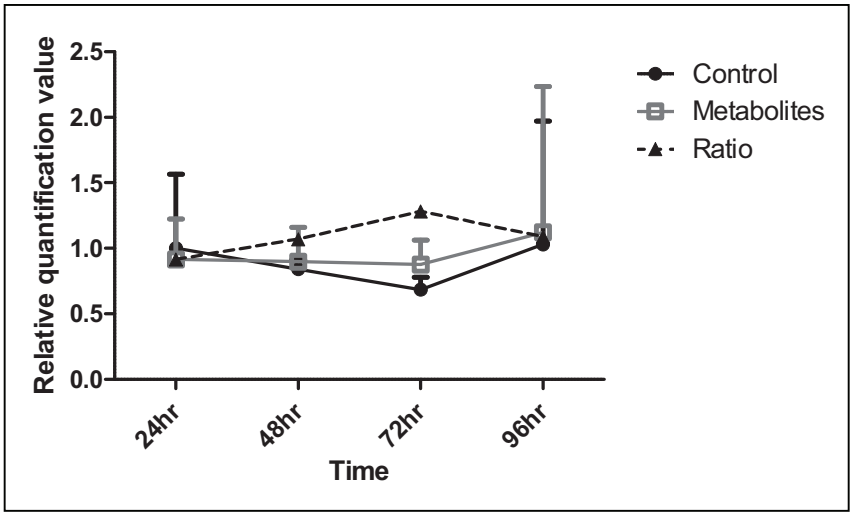

Figure 5-3. Expression of *ERCC1* by Hepg2 cells after exposure to a combination of 50 µM SA and 100 µM pHPPA. The solid black line indicates relative expression of *ERCC1* in control cells; the solid grey line indicates relative expression *ERCC1* in metabolite treated cells; the dashed black line indicates ratio between gene expression in control and metabolite treated cells. Relative quantification values are mean values for 3 biological repeat experiments done in triplicate. Error bars represent relative quantification maximum values as calculated to 2 standard deviations of mean.

The expression levels of *ERCC1* then seem to hold steady with only a slight decrease of 5% between 24 h and 72 h incubation time in the presence of the metabolites. However, this decrease is less than the decrease in control cells and results in a slightly higher expression of *ERCC1* in metabolite treated cells compared to control cells. Between 72 h and 96 h, the relative level of *ERCC1* expression in metabolite treated cells mimics the expression in control cells, but is only less pronounced.

Overall, an increase of approximately 20% is seen in the relative expression of *ERCC1* between 24 h and 96 h metabolite exposure. At first it may seem as if the relative expression of *ERCC1* in control and metabolite treated cells follow the same pattern, i.e. an initial decrease between 24 h and 72 h, followed by an increase between 72 h and 96 h. A two-way ANOVA, however, again reveals that neither metabolite treatment nor time has a significant effect (significance: $p<0.05$) on *ERCC1* expression. Similar to *hOGG1*, *ERCC1* expression also varies intra- and inter-individually (Brabender *et al.,* 2008:1815, Vogel *et al.,* 2002:1505, Woelfelschneider *et al.,* 2008:1758). Once again, the high degree of standard deviation observed may be a reflection of this variability.

These observations together with the observed decrease in NER capacity after 48 h metabolite exposure (van Dyk *et al.,* 2010:32) suggests that the metabolites probably either affect ERCC1 on protein functionality level rather than an expression level, or that a protein other than ERCC1, also involved in the initial steps of NER, is affected.

To determine which of the two metabolites, SA or pHPPA, had the largest contribution to the observed effects on relative *hOGG1* and *ERCC1* expression levels, HepG2 cells were incubated with either 50 µM SA or 100 µM pHPPA for 48 h. RNA was extracted from these cells and the relative expression of the genes determined by real-time PCR. The gene expression levels were once again calculated relative to the expression levels of *18S*. The expression level of *hOGG1* and *ERCC1* in control cells were normalised to one and the gene expression levels in metabolite treated cells calculated relative to the control values. Results for *hOGG1* and *ERCC1* expression levels are given in figure 5-4.

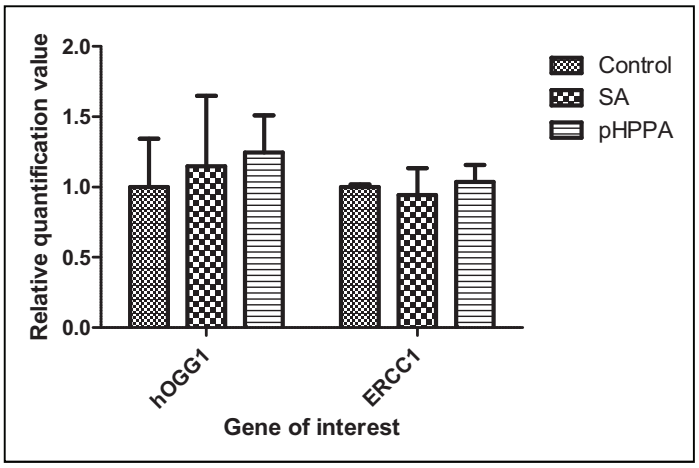

Figure 5-4. Expression of *hOGG1* and *ERCC1* by HepG2 cells after exposure to SA or pHPPA seperately. Relative quantification values are mean values for 3 technical repeats. Error bars indicate standard deviation.

The relative quantification values of *hOGG1* after exposure, to either SA or pHPPA for 48 h, show a slight increase in *hOGG1* expression. The expression of *hOGG1* increased by 14% after exposure to SA and increased by 25% after exposure to pHPPA. The slight increase seen here (figure 5-4) is, however, not significant.

The above, together with the similar pattern of expression in control and metabolite treated cells seen in figure 5-2, and the large standard deviations that were observed, indicate that the changes in *hOGG1* expression, seen in both of the experiments, are not due to effects of the metabolites on gene expression, but rather due to natural variation in *hOGG1* expression (Hanaoka *et al.,* 2000:1255). Hence, the metabolites do not seem to effect expression of *hOGG1* directly.

Exposure to either SA or pHPPA caused only very small changes in *ERCC1* expression. These results confirm the earlier observation (figure 5-3) that the metabolites do not significantly affect the expression of *ERCC1*. This also confirms the earlier suggestion that the observed decrease in NER capacity (van Dyk *et al.,* 2010:32) is either due to a direct effect of the metabolites on the functionality of ERCC1, or alternatively that one (or more) of the other proteins involved in damage recognition and excision is affected, or that protein-protein interactions of NER are influenced.

One such protein that might be affected is XPF, which forms a complex with ERCC1, and this complex then carries out the 5' incision (Christmann *et al.,* 2003:3). ERCC1 and XPF is furthermore unstable in the absence of each other (Friedberg *et al.,* 2006:1118). If either of ERCC1 or XPF is therefore affected, the 5' incision cannot be made. Another protein that might be affected is XPG, which performs the 3' incision (Christmann *et al.,* 2003:3). The 3' incision and the 5' incision occurs almost simultaneously (Friedberg *et al.,* 2006:1118). Therefore, if any one of these 3 proteins is affected, either through lowered gene expression or alteration of protein functionality, a lowered DNA repair capacity, (as seen with the comet assay (van Dyk *et al.,* 2010:32)), would be observed.

These observations are, however, made after exposure of cells to selected metabolites for a relatively short period. General limitations for the use of cell cultures, such as effects of confluency and 'out of tissue context' may influence results when using cell cultures for long term exposure to the metabolites.

As will be discussed in chapter 9, a mutator phenotype is frequently proposed as the mechanism by which cancers develop (Bielas and Loeb, 2005:206, Bielas *et al.,* 2006:18238, Bignold, 2004:299, Karpinets and Foy, 2005:1323, Kunkel, 2003:105, Loeb *et al.,* 1974:2311, Loeb *et al.,* 2008:3551, Pang *et al.,* 2006:157, Venkatesan *et al.,* 2006:294), and one of the contributors to the development of a mutator phenotype is deficient DNA repair mechanisms. Currently, no information is available on the expression levels of DNA repair proteins in HT1 patients. The level of expression of *hOGG1* and *ERCC1* was therefore assessed in HT1 patients. Results of the expression of *hOGG1* and *ERCC1*, as well as *fah*, in the control person and each of the patients are given in figure 5-5.

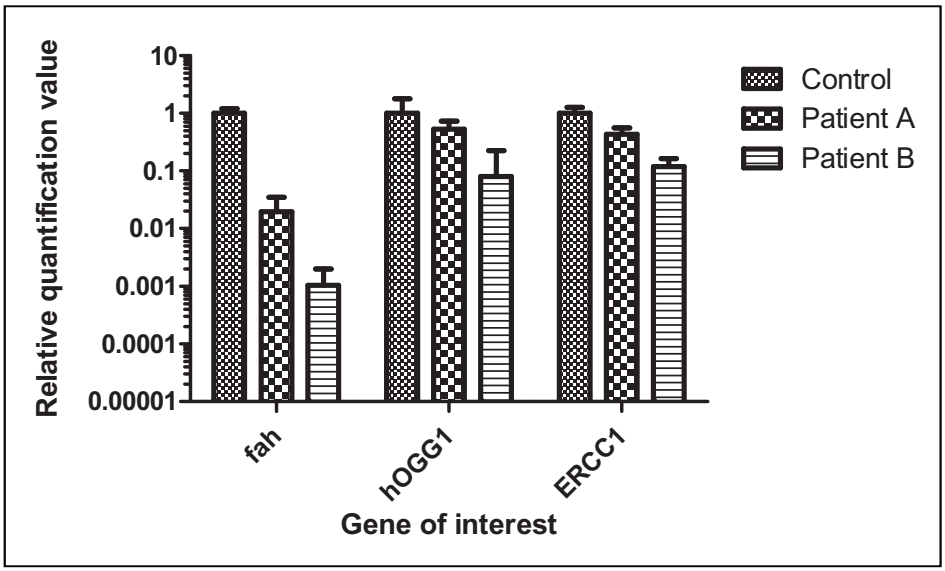

Figure 5-5. Expression of *fah, hOGG1* and *ERCC1* by control and patient primary lymphocytes. Due to limited sample availability, relative quantification values are mean values for 3 technical repeats. Error bars represent standard deviation.

Similar to the processing of the data of the previous gene expression experiments, the expression levels of all the genes of interest relative to expression levels of *18S* in control samples are normalised to one. It is important to note that the very large difference in relative quantification values between *fah* expression in the lymphocytes of control and patient samples prompted the use of a semi-logarithmic presentation of the results. From figure 5-5 it is apparent that patient A showed less than 2% and patient B less than 1% *fah* expression compared to the control person. These results confirm the diagnosis of HT1 in both patients. The expression of *hOGG1* and *ERCC1* are also low in both patients. Compared to expression of *hOGG1* control cells, expression of the gene is approximately 53% in patient A and 8% in patient B. The relative expression of *ERCC1* follows the same trend, with patient A having approximately 43% expression and patient B 12% expression. The similar low expression of *hOGG1* and *ERCC1* in each patient, is consistent with the observation by Vogel and colleagues that the mRNA levels of these genes are closely correlated. They speculated that *hOGG1* and *ERCC1* might be regulated by the same factors (Vogel *et al.,* 2002:1505). Although the observed differences in *hOGG1* and *ERCC1* expression between control and HT1 samples may be attributable to inter-individual variation, the expression levels of *hOGG1* and *ERCC1* are closely correlated with the BER and NER capacity of cells (Hodges and Chipman, 2002:55, Langie *et al.,* 2007:302, Lee *et al.,* 2004:9857, Vogel *et al.,* 2000:197), which implies that low mRNA expression of *hOGG1* and *ERCC1* is associated with reduced BER and NER capacity.

The low expression of *hOGG1* and *ERCC1* in HT1 patients, coupled with the effect of accumulating metabolites on the protein functionality of BER and NER proteins (van Dyk *et al.,* 2010:32), suggests that the capacity of HT1 cells for DNA repair are severely affected. Not only is

the expression of the repair proteins low, the functionality of the proteins that are expressed are diminished by the accumulating metabolites. This diminished capacity for DNA repair may contribute to the development of a mutator phenotype in HT1.

5.3 Genome stability

The correlation frequently found between genome stability and carcinogenesis, highlights the importance of genome integrity and stability maintenance (Charames and Bapat, 2003:589, Jackson, 2002:687, Mitra *et al.,* 2002:15). In a broad sense genomic instability can be divided into chromosomal instability, microsatellite instability and point mutation instability (Charames and Bapat, 2003:589, Bielas *et al.,* 2006:18238). Chromosomal instability refers to the mis-segregation of genetic information, whereas microsatellite instability refers to the addition or subtraction of the repeat sequences of microsatellites (Charames and Bapat, 2003:589, Buhard *et al.,* 2006:241). Point mutation instability is the increase of random point mutations (Bielas *et al.,* 2006:18238). MSI is distinct from allelic imbalance and observed loss of heterozygosity (Boland *et al.,* 1998:5248). The association between MSI and carcinogenesis led to the frequent use of MSI to identify tumours (Bacher *et al.,* 2004:237, Demokan *et al.,* 2006:995, Macdonald *et al.,* 1998:90, Salvucci *et al.,* 1999:181, Samowitz *et al.,* 2001:1517). However, MSI testing has also been used to determine the effect of hypoxia or aging on mismatch repair pathways and therefore genome stability (Lee *et al.,* 2010:83, Neri *et al.,* 2004:499).

It was suggested that cancer develops through either a chromosomal instability mutator phenotype (CIN) or a microsatellite instability mutator phenotype (MIN), and the choice is driven by the type of carcinogen (Bardelli *et al.,* 2001:5770, Breivik and Gaudernack, 1999:245). However, Trautmann and colleagues have shown that CIN and MIN are not mutually exclusive in colon cancer (Trautmann *et al.,* 2006:6379). Several reports have shown the presence of chromosomal instability, i.e. chromosomal breakage, aneuploidy, spindle disturbances and segregational defects, in HT1 (Gilbert-Barness *et al.,* 1990:243, Jorquera and Tanguay, 2001:1741, Zerbini *et al.,* 1992:1111). However, no MSI has been reported in HT1. Therefore, the observations that MSI is a marker of a mutator phenotype, and deficiency of DNA repair is one of the contributing factors to the development of a mutator phenotype (Loeb, 1994:5059), together with the diminished DNA repair capacity of HT1 cells reported in sections 5.1 and 5.2, prompted the investigation into the occurrence of MSI in HT1.

MSI was analysed in DNA samples from the *fah*$^{-/-}$ mouse model. DNA was isolated from liver of a control mouse, a *fah*$^{-/-}$ mouse continuously on NTBC and a FAH$^{-/-}$ mouse of NTBC for 40 days. Although 40 days seem limiting, it was reported that this time interval was enough to elicit an

ER stress response (Bergeron *et al.,* 2006:5329), and cause progressive liver and kidney pathophysiology (Orejuela *et al.,* 2008:308). Also, without NTBC treatment the *fah* deficient mice die within four to eight weeks (Luijerink *et al.,* 2003:901). Microsatellite markers as described by Zhang and colleagues (Zhang *et al.,* 2004:521) were used to determine microsatellite instability. The specific microsatellite markers were chosen as it was reported that genomic instability in mouse chromosomes 3, 7, 11 and 16 has a role in the development and progression of HCC in mice (Zhang *et al.,* 2004:521). The markers and relevant information are given in table 5-2.

Table 5-2. Information on microsatellite markers used for MSI testing in mouse DNA.

Marker	Position (cM)	Human homology region
D3Mit21	14.2	3q24-q28
D7Mit18	25.1	11p15-p14
D7Mit10	62.3	10q24-q26
D11Mit7	40.4	17p13

(Zhang *et al.,* 2004:521)

The results of the MSI analyses, after amplification of markers by conventional PCR and separation of the amplicons on a DNA 1000 chip from Agilent on a 2100 Bioanalyzer (Odenthal *et al.,* 2009:850), are presented in figure 5-6.

Marker	Electrophoretogram
D3Mit21	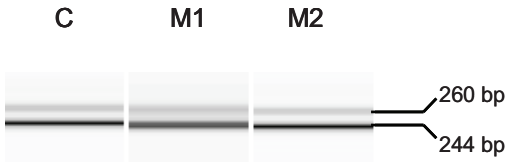
D7Mit18	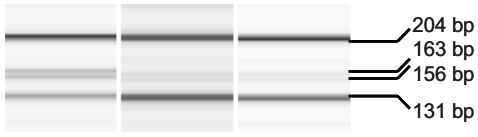
D7Mit10	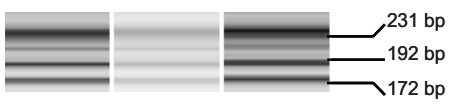
D11Mit7	

Figure 5-6. Microsatellite analysis of mouse DNA. C: *fah*$^{+/+}$ control mouse; M1: *fah*$^{-/-}$ mouse constantly on NTBC; M5: *fah*$^{-/-}$ mouse off NTBC for 40 days.

A similar microsatellite amplification pattern is obtained for each of the microsatellite markers, when comparing the microsatellite amplification pattern in the control mouse and the microsatellite amplification pattern from the mice constantly on or off NTBC treatment for 40 days. The only slight difference that is observed is in the amplification profile of D7Mit18. In the control mouse the intensity of the largest fragment (204 bp) is the highest, with the three smaller fragments (131, 156, 163 bp) showing comparable intensities. In both of the *fah*$^{-/-}$ mice, the smallest (131 bp) and largest (204 bp) fragments have similar intensities, and the two mid-sized fragments (156 and 163 bp) have much lower intensities. This observed change might be the result of allelic imbalance occurring.

Allelic imbalance is a molecular characteristic of chromosomal imbalance, and is regular trait in tumours such as HCC (Aihara *et al.,* 1998:86, Zhang *et al.,* 2004:521). Zhang *et al.,* suggested that chromosomes 3, 7, and 11 carry tumour suppressor genes and are key to the development of HCC in mice (Zhang *et al.,* 2004:521). Although the sample size is small, the observed change in intensity of the D7Mit18 fragments could be an indicator of chromosomal imbalance and may point to the development of HCC in the *fah*$^{-/-}$ mice, which would be in line with the observations by Al-Dhalimy *et al*. that HCC develops in *fah* deficient mice even with dietary intervention and pharmacological treatment (Al-Dhalimy *et al.,* 2002:38, Mitchell *et al.,* 2001:1777).

To determine the effect of the accumulating metabolites on the human genome, HepG2 cells were exposed to a combination of SA and pHPPA for 72 h. DNA was isolated and genomic stability analysed, via amplification of microsatellite DNA by conventional PCR and separation of the PCR products on a DNA 1000 chip from Agilent on a 2100 Bioanalyzer. A selection of 5 microsatellite markers, as recommended by the Bethesda reference panel, was used to assess the genomic stability in the metabolite-exposed cells compared to unexposed control HepG2 cells.

Table 5-3. Microsatellite repeat motifs.

Marker	**Location**[1]		**Repeat motif**[2]
	Chromosome	**Gene**	
BAT25	4q12	*c-kit*	TTTT.T.TTTT.$(T)_7$.A$(T)_{25}$
BAT26	2p16	*hMSH2*	$(T)_5$…..$(A)_{26}$
D2S123	2p16	*hMSH2*	$(CA)_{13}TA(CA)_{15}(T/GA)_7$
D5S346	5q21	*APC*	$(CA)_{26}$
D17S250	17q11	*BRCA1*	$(TA)_7$……$(CA)_{24}$

[1]Information on microsatellite marker location from House et al. (House *et al.,* 2003:902).

[2]Repeat motifs are from Dietmaier et al., (Dietmaier *et al.,* 1997:4749). Dots represent non-repetitive nucleotides.

The panel of markers include two mononucleotide repeats BAT25, BAT26, and three dinucleotide repeats D2S123, D5S346, and D17S250 (Boland *et al.,* 1998:5248). Repeat motifs and relevant information of these markers are given in table 5-3.

Results from the genomic stability analyses in metabolite exposed HepG2 cells are given in figure 5-7.

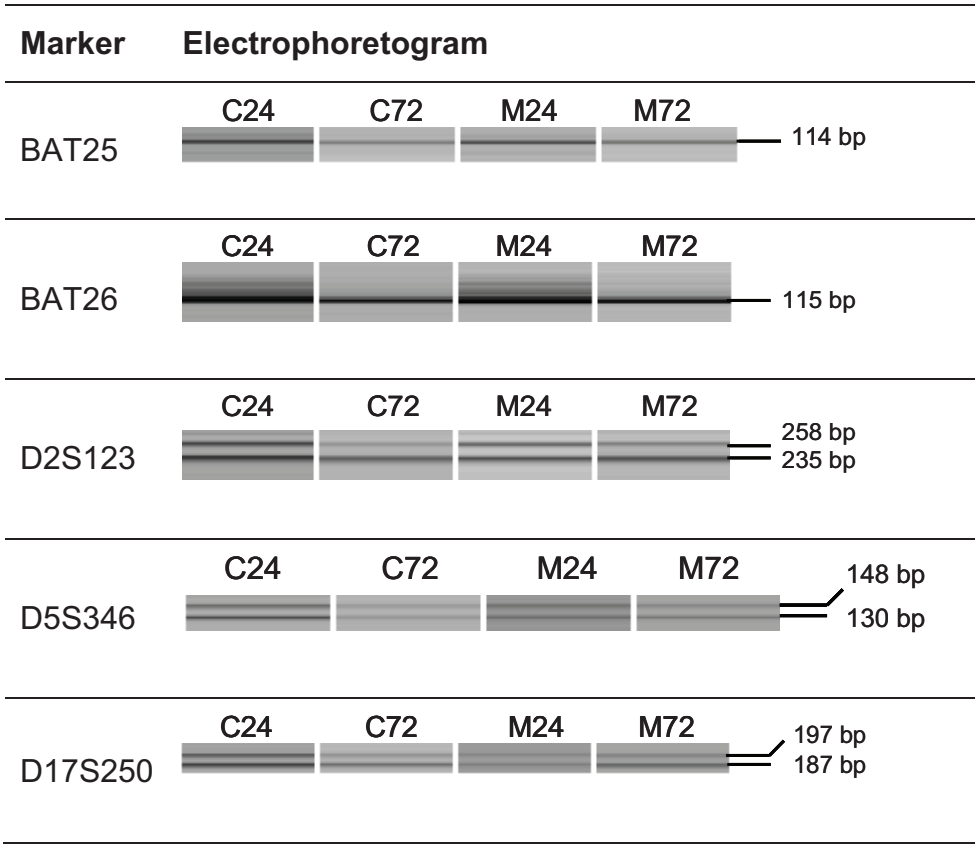

Figure 5-7. Electrophoretograms of the different microsatellite markers. C24: Control HepG2 cells after 24 h; C72: Control HepG2 cells after 72 h; M24: HepG2 cells treated with metabolites for 24 h; M72: HepG2 cells treated with metabolites for 72 h.

From the results in figure 5-7, it is clear that, for all of the selected microsatellite markers, no variation is observed, i.e. microsatellite DNA from HepG2 cells exposed to SA and pHPPA for 72 h shows no variation from microsatellite DNA from unexposed control HepG2 cells. Also, no allelic imbalance is observed in the HepG2 cells exposed to the metabolites. These results indicate that short term exposure of HepG2 cells to SA and pHPPA does not affect genome stability, either through microsatellite instability or allelic imbalance, as measured by MSI testing.

As the gene expression level of DNA repair proteins was diminished in lymphocytes of HT1 patients, the reduced DNA repair capacity in these cells might result in genetic instability in the lymphocytes. In individuals of Eurasian origin, BAT25 and BAT26 are quasimonomorphic, i.e. small size differences of no more than 1 or 2 basepairs (Buhard *et al.,* 2006:241) occur, making

direct comparison between control and patient samples possible. However, dinucleotide repeats, such as CA repeats, may have different alleles in a population (Richards and Hawley, 2011:172). More than one control was therefore included in the study to compensate for inter-individual variability that may exist in the dinucleotide repeats. The microsatellite analysis results after separation on a DNA 1000 chip from Agilent is given in figure 5-8.

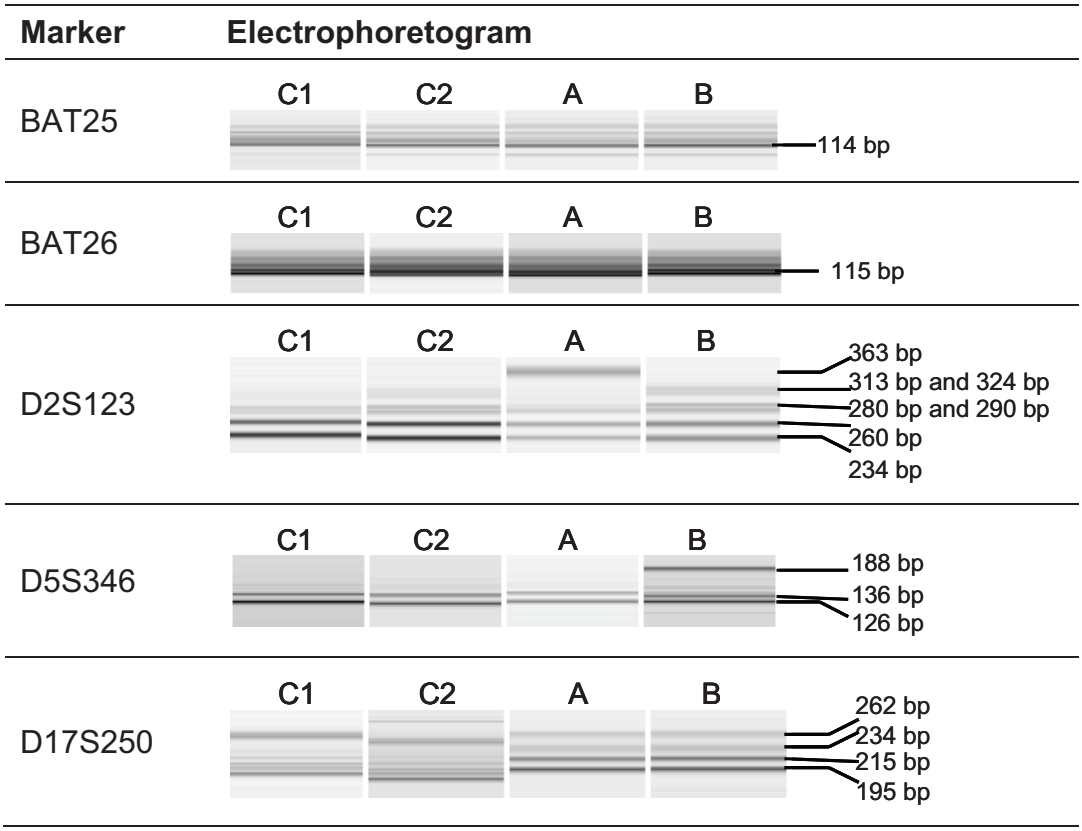

Figure 5-8. Microsatellite analysis of the five microsatellite markers as recommended by the Bethesda panel. C1: control person 1; C2: control person 2; A: Patient A; B: Patient B.

From figure 5-8 it is clear that for both of the mononucleotide repeats, BAT25 and BAT26, no variance is observed between patient and control samples, i.e. the microsatellite amplification pattern is the same. Similar amplification patterns of D2S123 are also observed for controls and patient B. (Although the larger bands of approximately 313 and 324 bp are not clearly visible in control 1, the bands are present). For patient A, however, a slightly altered amplification pattern is observed. Similar to controls 1 and 2 and patient B, bands of approximately 234, 260, 280, 290 bp is seen for patient A. However, the 313 and 324 bp bands are absent; instead a larger band of 363 bp is seen. Unlike controls 1 and 2 and patient B, where the smallest bands are the most prominent, in patient A the largest band is the most prominent.

The microsatellite amplification pattern of the dinucleotide D5S346 is similar for controls and patient A. Bands of approximately 126 and 140 bp are observed. In patient B, this

microsatellite amplification profile is slightly different with bands of 126, 136, 152 and 188 basepairs.

For the D17S250 dinucleotide repeat the biggest variation in the microsatellite amplification pattern is observed. Although the amplification bands are slightly smaller in control 2 compared to control 1, the same pattern is observed. For both controls, six bands can be distinguished, with the largest and smallest bands the most prominent. When compared to the controls, the microsatellite amplification pattern of D17S250 is different in the patients. In both patient A and patient B, only four amplification bands are present. Furthermore, unlike the controls, in the patients the two smallest bands have the highest intensity.

To summarise, no variance is observed in the mononucleotide repeats, BAT25 and BAT26, between control and patient samples. However, differences between control and patient samples are observed for dinucleotide repeats. Patient A differs from controls at the D2S123 and D17S250 dinucleotide repeats, and patient B differs from controls at the D5S346 and D17S250 dinucleotide repeats.

Interestingly, when comparing patient A to patient B, different amplification patterns were obtained for the D2S123 and D5S346 dinucleotide repeats, but a similar pattern was obtained for the D17S250 dinucleotide repeat. Keeping in mind that the two HT1 patients are siblings and that sequence length variation is inherited in a co-dominant Mendelian way (Srikwan *et al.,* 1996:267) and since the D2S123 marker pattern of patient B is similar to controls, it suggests that the altered pattern seen in patient A is novel to patient A and not inherited. Similarly, the altered pattern of D5S346 in patient B might be novel to patient B. The similarity of the microsatellite amplification pattern of D17S250 between the patients but dissimilarity to the microsatellite amplification pattern in the controls, could be novel microsatellite instability in both of the patients, but might also be because of the high degree of allele variability that exists for dinucleotide repeats (Odenthal *et al.,* 2009:850). As the D7Mit18 marker indicated possible allelic imbalance in the *fah* deficient mice, the fragment intensity changes, seen with the D17S250 marker in the patients, might also reflect allelic imbalance. However, as it is not clear whether the D17S250 MSI in the HT1 patients is due to novel microsatellite instability or because of the stated high allele variability for dinucleotides, it is difficult to be certain if the D17S250 intensity changes observed in the patients are truly due to microsatellite imbalance.

Tumours are regarded as MSI-H (high frequency of MSI) when two or more of the microsatellite markers show instability, MSI-L (low MSI frequency) when one of the markers shows instability and MSS (microsatellite stable) when no instability is found (Boland *et al.,* 1998:5248). Although the microsatellite DNA analysed in the HT1 patients were from non-tumour DNA, it is interesting to note that if the above mentioned criteria for tumour MSI classification is used, both

patients would be classified as MSI-L, and possibly even MSI-H, as instability is observed for one (maybe two) of the five markers tested.

Several reports have described microsatellite instability analyses as an useful method to determine defective DNA mismatch repair (Buhard *et al.,* 2006:241, Dietmaier *et al.,* 1997:4749, House *et al.,* 2003:902, Macdonald *et al.,* 1998:90, Maehara *et al.,* 2001:249). The presence of MSI in the lymphocytes of the HT1 patients, could therefore, albeit indirectly, suggest that in addition to the decreased capacity for base- and nucleotide repair by HT1 cells (van Dyk *et al.,* 2010:32), the capacity of HT1 cells for DNA mismatch repair might also be affected.

It is interesting to speculate on the possible involvement of DNA methyltransferase 1 (DNMT1). In a study by Guo and colleagues (Guo *et al.,* 2004:891) they identified DNMT1 as a novel gene involved in mismatch repair. They also found that cells deficient in DNMT1 activity had a four times higher CA dinucleotide slippage rate, compared to wild-type cells. Simultaneously, Kim and colleagues (Kim *et al.,* 2004:5742) found that DNMT1 deficient cells had a seven-fold increase in mononucleotide microsatellite slippage rate. In a study in our laboratory, Mr Jean du Toit found with the cytosine extension assay that DNA from the HT1 patients had global DNA hypomethylation (publication in progress). Results from this assay, courtesy of Jean du Toit, are given in figure 5-9.

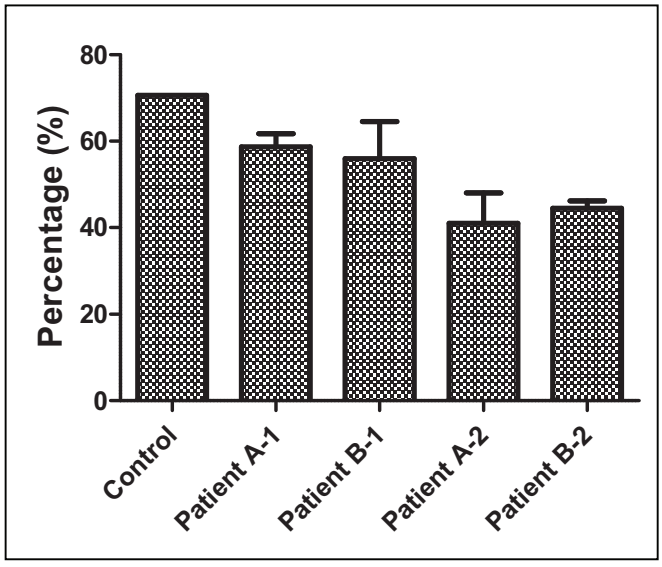

Figure 5-9. DNA methylation in control and HT1 patients. Results are mean values for three separate experiments. Error bars represent standard deviation.

From these results the global demethylation seems to be progressive, as DNA samples 1 and 2 from the HT1 patients were taken about 8 months apart. DNMT1 activity is traditionally linked to the conservation of methylation patterns (Wilson *et al.,* 2007:138). The global

hypomethylation seen in the HT1 patients could therefore point to a possible deficiency of DNMT1. Keeping all the above in mind, one could speculate that MSI and hypomethylation seen in the HT1 patients is causally linked through deficient DNMT1 activity. One may further speculate that the deficiency of DNMT1 could be the result of interference by succinylacetone, as the regulatory and catalytic regions of DNMT1 are linked by a series of lysine-glycine repeats (Pradham *et al.,* 2008:10000), and these amino acids are the most reactive with SA (Manabe *et al.,* 1985:1060).

To summarise, results show the occurrence of allelic imbalance on chromosome 7 of the *fah*$^{-/-}$ mouse genome, confirming previously reported chromosomal instability in HT1 (Gilbert-Barness *et al.,* 1990:243, Jorquera and Tanguay*,* 2001:1741, Zerbini *et al.,* 1992:1111). Incidentally, the observation of instability of specifically the D7Mit18 microsatellite marker, indicates the possible involvement of the growth arrest specific 2 (*gas2*) and *ras* genes in HT1. The D7Mit18 marker is located in the *gas2* gene, and according to the Entrez gene summary of this gene, high levels of this gene is associated with growth arrested cells. Instability of this gene could therefore be one of the contributing factors of the cell cycle arrest seen in HT1 (Bergeron *et al.,* 2006:5329, Vogel *et al.,* 2004:433). At the same time, D7Mit18 is located 1.9cM from *ras* (Zhang *et al.,* 2004:521), a cancer associated gene (Lumniczky *et al.,* 1998:100), suggesting the possible involvement of *ras* in the development of HCC in HT1.

The results furthermore show instability of the D2S123, D5S346 and possibly the D17S250 microsatellite markers. Loeb (Loeb, 1994:5059) hypothesized that alterations in the genetic stability genes (i.e. genes involved in DNA replication, DNA repair, chromosomal segregation etc) could lead to relaxed genomic stability and could be the generator of multiple mutations that are observed in tumours. As these markers are located in the *hMSH2*, *APC* and *BRCA1* genes respectively, the observed instability of these genes may point to early events in the carcinogenic process in HT1. Put differently, instability of these genes could lead to relaxed genomic stability, which leads to the development of a mutator phenotype, which results in the observed HCC in HT1.

More importantly, it is possible that the low expression of the DNA repair proteins (and by extension, a low DNA repair capacity) is a contributing factor to the observed genetic instability seen in the lymphocytes of the HT1 patients. In the liver of HT1 patients, the same type of situation might occur, only more severe. In HT1 hepatocytes, the mutagenicity of FAA (Jorquera and Tanguay*,* 1997:42), could place an additional burden on the already decreased DNA repair capacity of the cell. As HT1 cells are also resistant to cell death (Orejuela *et al.,* 2008:308), mutations may accumulate. The accumulation of mutations may then contribute to the development of HCC, seeing as HCC, like most solid tumours, develops and progresses through the accumulation of several genetic changes (Saffroy *et al.,* 2004:649).

5.4 Point mutation instability

As speculated in foregoing sections, the observed decreased DNA repair capacity may result in the accumulation of mutations. Therefore, high resolution melting (HRM) and subsequent sequencing of selected parts of the *fah* and *hprt1* genes were performed, to determine if *de novo* mutations occurred. HRM is a novel, rapid, accurate and inexpensive technique used in a wide range of applications such as mutation discovery (gene scanning), screening for loss of heterozygosity, and somatic acquired mutation ratio, etc (Taylor, 2009:433). This technique is based on the effect of DNA base changes on the melting temperature (T_m) of a DNA duplex fragment (Liew *et al.,* 2004:1156, Taylor, 2009:433). Both homozygous and heterozygous sequence variants can be detected by HRM as a homozygous change of a base pair (between A:T or G:C) in the DNA duplex changes the T_m of the DNA duplex between 0.8 - 1.4℃ (Liew *et al.,* 2004:1156) and heterozygous changes alter the melting curve shape (Taylor, 2009:433). However, when the base pair is unchanged and the bases only switch strands the T_m change are smaller (<0.4℃) or undetectable (Liew *et al.,* 2004:1156, Taylor, 2009:433). Although HRM was successfully performed on amplicons sized between 38 and 1000 bp, DNA duplex fragments of the size range 100 – 300 bp is preferred, since T_m changes is greater and more readily detected in smaller fragments (Taylor, 2009:433). Third generation intercalating DNA-dyes such as LCGreen®, SYTO®9 and Eva Green™ are used for HRM, as these dyes have low toxicity and can be used at higher concentrations to saturate available binding sites at a concentration compatible with PCR (Taylor, 2009:433, Wittwer *et al.,* 2003:853).

Genomic DNA was isolated from whole blood of the two HT1 patients. A 105 bp fragment from exon/intron 12 on human *fah*, and a 117 bp fragment from exon 3 on human *hprt1* were amplified by PCR. These amplicons were then analysed by HRM and sequencing. Although the liver is the main affected organ in HT1 (Berger, 1996:107, Bergeron *et al.,* 2001:15225), the genetic instability observed in the lymphocytes of the HT1 patients suggests that accumulation of mutations may also be observed in the lymphocytes.

Additionally, three fragments (89, 97 and 113 bp) from the mouse *hprt1* gene were analysed by HRM. DNA isolated from control and *fah*$^{-/-}$ mice was used. The PCR product from one of these fragments (HPP4: 97 bp) obtained after both conventional PCR and COLD-PCR was inserted into the pEZSeq™ HC Amp vector and sequenced by dideoxy sequencing with the Z-for primer in the forward direction.

Fah and *hprt1* were chosen as target sites for HRM and sequencing, because *fah* is the gene that is mutated in HT1 and *hprt1* is frequently used to determine mutation frequency (Albertini, 2001:1, Albertini *et al.,* 2010:77, Coryell and Stearns, 2006:114, Tereshchenko *et al.,* 2010:551). The specific *fah* and *hprt1* fragments were chosen, because when the complete *fah*

and *hprt1* genes are considered, there is a higher proportion of reported disease causing mutations in these areas, compared to the rest of the gene (fig 2-2 and 5-10). Also, the *fah* DNA fragment includes the location of two mutations that is known to revert.

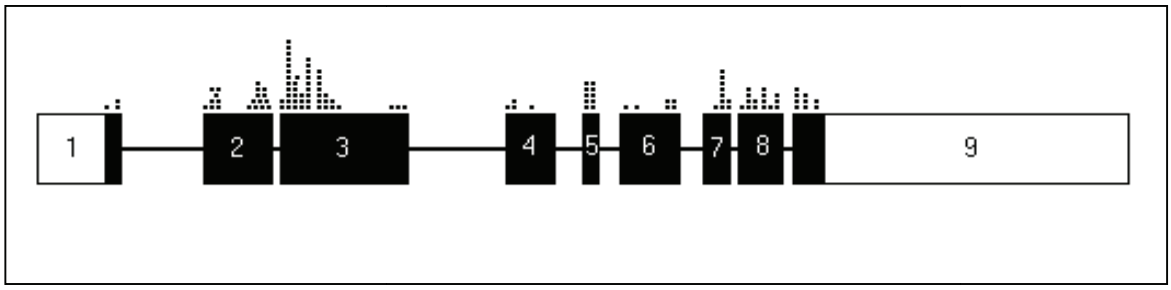

Figure 5-10. Position of Lesch-Nyhan disease causing mutations on the human *hprt1* gene. Boxes indicate exons and connecting lines indicate introns. Coding regions is shaded in black. Black squares on top of gene indicate location single base alterations. (Adapted from Jinnah *et al.,* 2001:1).

Results obtained from HRM of *fah* DNA fragments are normalised against fluorescence. The normalised melting curves, for control and patient *fah* 105 bp amplicons, are shown in figure 5-11.

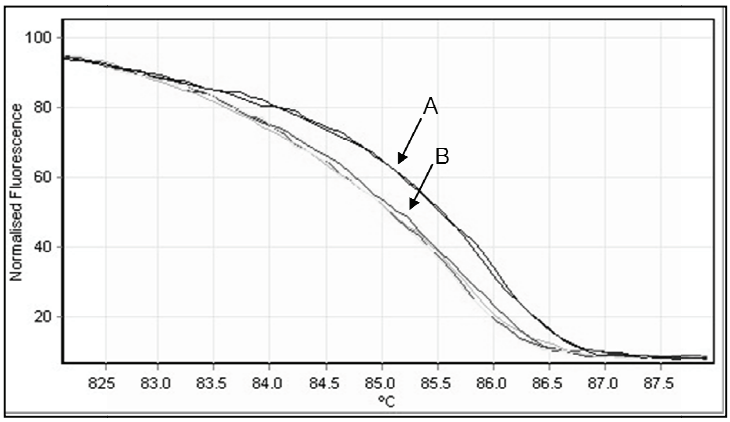

Figure 5-11. Fluorescence-normalised melting data from HRM of human *fah* amplicons. A: Melting curve of control amplicons. B: Melting curve of amplicons from patient DNA.

At 60% fluorescence the melting temperature of the DNA fragments amplified from patient DNA (A) is approximately 0.5℃ lower than fragments amplified from control DNA (B). The shape of the curves is similar, which removes the possibility of a heterozygous base change. To determine if the change in T_m is due to a change in the sequence, the amplicons were sequenced via dideoxy sequencing in forward and reverse orientations.

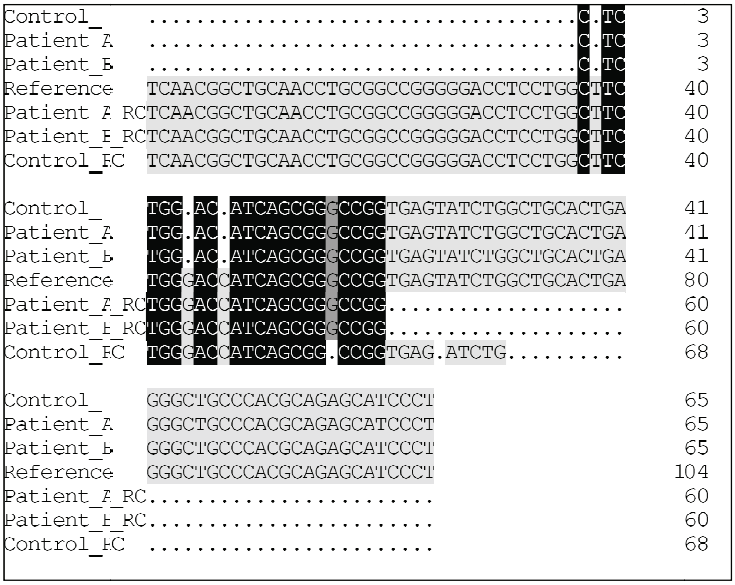

Figure 5-12. Multiple aligned *fah* sequencing results. Control: Forward sequence from control DNA. Patient A: Forward sequence from patient A. Patient B: Forward sequence from patient B. Reference: Reference sequence (NM_000137.2). Patient A_RC: Reverse complement sequence from patient A. Patient B_RC: Reverse complement sequence from patient B. Control RC: Reverse complement sequence from control. White text on black background indicates complete sequence similarity between all sequences. Black text on grey background indicates sequence similarity between more than 50% of the sequences.

Analyses of the forward and reverse complement sequencing results from the human *fah* fragments revealed no sequence variation between control and patient *fah* fragments (figure 5-12). There is also no sequence variation when compared to the reference sequence (*fah*, NM_000137.2). Disparity between the patient sequences and the control or reference sequence in one orientation is refuted by the sequence results from the second orientation.

The difference between the results of HRM and sequencing may lie in the sensitivity of the two techniques. Dideoxy sequencing is rarely sensitive below 10% mutant allele frequency, in other words when sequencing, for instance tumour DNA, the sequence change must be present in at least 10% of the tumour cells to be detectable by dideoxy sequencing of the whole genome (Klein, 2006:18033). On the other hand, the sensitivity of HRM can be as low as 5% (very good) when analysing fragments shorter than 100bp (Krypuy *et al.,* 2006:295). However, the above should not lead to the assumption that the T_m difference seen in the HRM analyses is conclusive of a different genotype. Together with characteristics of the DNA duplex, such as the sequence and/or the GC content, factors such as the ionic strength of the buffer solution, the presence of substances such as DMSO, non-uniformity across microtitre-format melting instruments, DNA isolation method and DNA concentration, influence the T_m of an amplicon (Owczarzy *et al.,* 2004:3537, Rouzina and Bloomfield, 1999:3242, Seipp *et al.,* 2007:284, Taylor, 2009:433).

Keeping all the above mentioned in mind, it is therefore unclear whether the observed T_m difference (figure 5-11) is an artefact of the experiment or if a sequence change has occurred, but is at a level that is undetectable via dideoxy sequencing.

In order to assess if the change in T_m was due to a change in sequence or the result of an experimental artefact, the *fah* fragment was amplified by COLD-PCR. The use of COLD-PCR instead of conventional PCR can result in a 5 to13 fold mutation enrichment (Li and Makrigiorgos, 2009:427). After amplification of the *fah* fragment by COLD-PCR, the amplicons were analysed by HRM. Results thereof, are presented in figure 5-13.

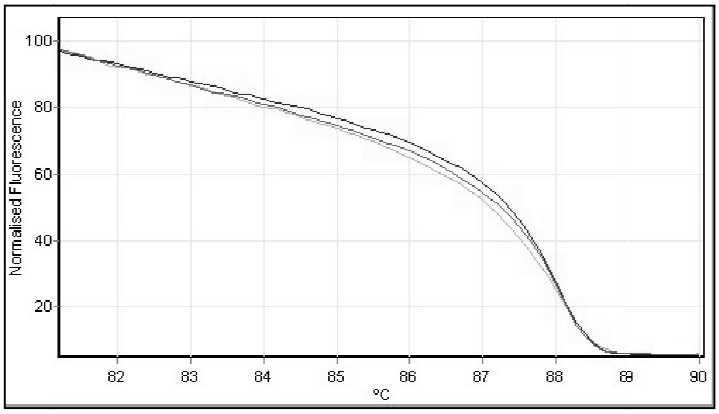

Figure 5-13. HRM results of the *fah* fragment, amplified by COLD-PCR. The high resolution melt curve of the control samples is represented by the light grey line. The black line represents the HRM curve of the patient A sample, and the dark grey curve line the patient B sample.

From the high resolution melt result of the *fah* fragment amplified by COLD-PCR, the T_m change observed in figure 5-11 seems to be the result of an experimental artefact, than the result of a change in sequence. This can be deduced from the observation in figure 5-13, that the melting curves of the control and patient *fah* fragments cluster together.

To determine if any *de novo* mutations occurred in other parts of the genome, *hprt1* was analysed. As mentioned, *hprt1* is frequently used as a reporter gene for the measurement of mutation frequencies. An increase in *hprt1* mutation frequency indicates that the exposure to mutagenic agents is having an effect (Albertini, 2001:1). The gene was analysed using HRM and dideoxy sequencing to establish if the long term exposure to accumulating metabolites caused mutations in the gene.

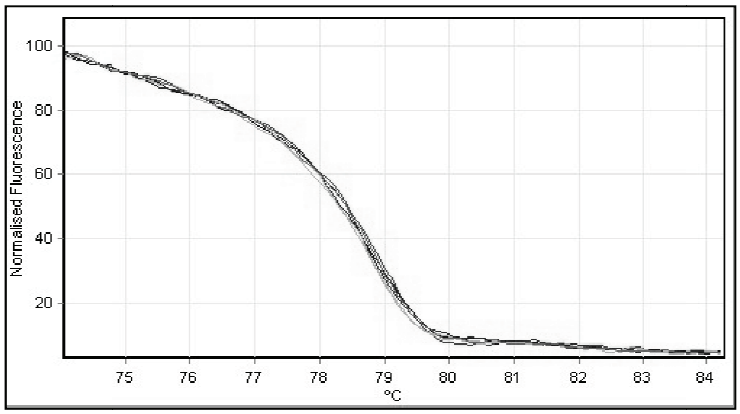

Figure 5-14. Fluorescence-normalised melting data from HRM of human *hprt1* amplicons.

Similar to HRM results of *fah*, results obtained after HRM of human *hprt1* fragments, are normalised against fluorescence (figure 5-14). All the normalised melt curves i.e. control and both patients, have comparable shapes, indicating that no heterozygous base pair changes have occurred. Also, no T_m changes that could indicate homozygous changes are observed. To confirm these results, all of the human *hprt1* fragments were sequenced via dideoxy sequencing. The results are given in figure 5-15.

```
Control_RC  ACTGAACGTCTTGCTCGAGATGTGATGAAGGAGATGGGAG     40
Patient_B_RCACTGAACGTCTTGCTCGAGATGTGATGAAGGAGATGGGAG     40
Patient_A_RC............GCTCGAGATGTGATGAAGGAGATGGGAG     28
Reference   ACTGAACGTCTTGCTCGAGATGTGATGAAGGAGATGGGAG     40
Patient_A   .....................................       0
Patient_B   .....................................       0
Control     .....................................       0

Control_RC  GCCATCACATTGTAGCCCTCTGTGTGCTCAA.........     71
Patient_B_RCGCCATCACATTGTAGCCCTCTGTGTGCTCAA.........     71
Patient_A_RCGCCATCACATTGTAGCCCTCTGTGTGCTCAA.........     59
Reference   GCCATCACATTGTAGCCCTCTGTGTGCTCAAGGGGGGCTA     80
Patient_A   ..CATCACATTGTAGCCCTCTGTGTGCTCAAGGGGGGCTA     38
Patient_B   ..CATCACATTGTAGCCCTCTGTGTGCTCAAGGGGGGCTA     38
Control     ..CATCACATTGTAGCCCTCTGTGTGCTCAAGGGGGGCTA     38

Control_RC  .....................................       71
Patient_B_RC.....................................       71
Patient_A_RC.....................................       59
Reference   TAAATTCTTTGCTGACCTGCTGGATTACATCAAAGCA      117
Patient_A   TAAATTCTTTGCTGACCTGCTGGATTACATCAAAGCN       75
Patient_B   TAAATTCTTTGCTGACCTGCTGGATTACATCAAAGCN       75
Control     TAAATTCTTTGCTCACCTGCTGCATTACATCAAAGCA       75
```

Figure 5-15. Multiple aligned human *hprt1* sequencing results. Control RC: Reverse complement sequence from control DNA. Patient B_RC: Reverse complement sequence from patient B. Patient A_RC: Reverse complement sequence from patient A. Reference: Reference sequence. Patient A: Forward sequence from patient A. Patient B: Forward sequence from patient B. Patient B: Forward sequence from patient B. White text on black background indicates complete sequence similarity between all sequences. Black text on grey background indicates sequence similarity between more than 50% of the sequences. Black text on white background indicates 33% sequence similarity.

Hprt1 fragments from control and patient DNA were sequenced in both forward and reverse orientation. Sequencing results from the forward sequencing orientation of the *hprt1* fragments amplified from both patients' DNA match both the reference sequence and the control sequence. The reverse compliment of the reverse *hprt1* sequence from patient B, matches the control and reference sequences for all but one base. The software called the last base an ambiguous N, but visual inspection of the chromatogram shows that an A can confidently be called. The *hprt1* fragment reverse compliment sequence from patient A is slightly truncated. Visual inspection of the chromatogram showed that in that part of the sequence the background was too high to be discarded and the sequence was therefore manually truncated. Similar to patient B, the ambiguous N at the last base may be called an A. The rest of the sequence is identical to the control and reference sequences. These results confirm the HRM results: that no changes are observed between *hprt1* fragments from control and patient DNA.

Three different *hprt1* DNA fragments, amplified by conventional PCR, from *fah*$^{-/-}$ mice permanently on or 40 days without NTBC, were analysed by HRM. Results obtained were normalised against fluorescence. Figure 5-16 depicts the results after HRM of one of the DNA fragments (HPP4: 97 bp). The other two fragments (HPP1: 89 bp and HPP5: 113 bp) gave similar results and the results can be found in appendix C.

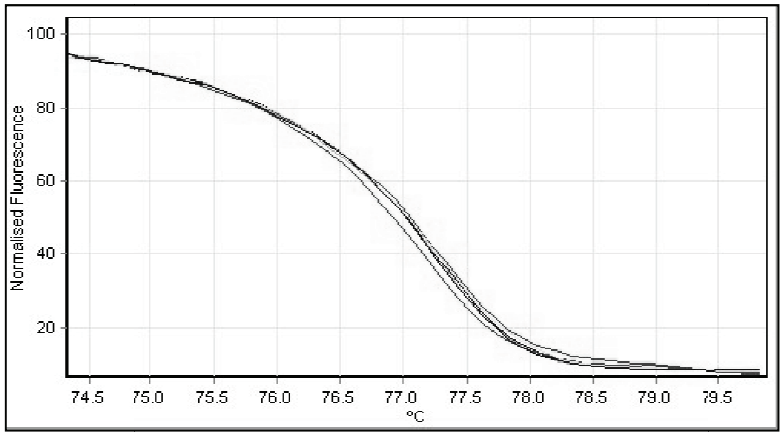

Figure 5-16. HRM results from the HPP4 fragment of mouse *hprt1.*

The high resolution melt curves of the mouse *hprt1* fragments amplified from DNA isolated from a control mouse and *fah*$^{-/-}$ mice continuously on, or 40 days off NTBC, are analogous in shape and T_m, indicating that no homozygous or heterozygous basepair changes occurred. However, since strand swapping of basepairs results in small or undetectable T_m changes, these sequence changes cannot yet be excluded.

To confirm the HRM results, the mouse *hprt1* fragments were sequenced after either conventional or COLD-PCR and insertion into pEZSeq™ HC Amp vector. Sequence results after conventional PCR are shown in figure 5-17.

Figure 5-17. Multiple aligned mouse *hprt1* sequencing results after conventional PCR. Control: Fragment sequence amplified from control mouse. Reference: Reference sequence (NM_013556.2). Mouse 5: Fragment sequence amplified from DNA from *fah*$^{-/-}$ mouse permanently on NTBC. Mouse 1: Fragment sequence amplified from DNA from *fah*$^{-/-}$ mouse off NTBC for 40 days. White text on black background indicates complete sequence similarity.

It is clear from figure 5-17 that the sequences of the *hprt1* fragments, amplified from DNA from a control mouse (control) and the *fah*$^{-/-}$ mice continuously on NTBC (mouse 1) or off NTBC for 40 days (mouse 5), show 100% sequence similarity to the corresponding reference sequence (NM_013556.2).

Figure 5-18. Multiple aligned mouse *hprt1* sequencing results after COLD-PCR. Reference: Reference sequence (NM_013556.2). Control: Fragment sequence amplified from control mouse. Mouse 1 (72): Fragment sequence amplified at 72℃ from DNA from *fah*$^{-/-}$ mouse permanently on NTBC. Mouse 5 (72): Fragment sequence amplified at 72℃ from DNA from *fah*$^{-/-}$ mouse off NTBC for 40 days. Mouse 5 (80): Fragment sequence amplified at 80℃ from DNA from *fah*$^{-/-}$ mouse off NTBC for 40 days. White text on black background indicates complete sequence similarity between all sequences.

The HPP4 *hprt1* fragments were also amplified by COLD-PCR. Results from sequencing of the different HPP4 *hprt1* fragments, after insertion into the pEZSeq™ HC Amp vector, are shown in figure 5-18.

HPP4 *hprt1* fragments were amplified by COLD-PCR at a T_c of 72℃ from control and *fah* deficient mice. The HPP4 *hprt1* fragment from the *fah*$^{-/-}$ mouse off NTBC for 40 days was also amplified by COLD-PCR at a T_c of 80℃. From figure 5-18 it is apparent that the sequences of all the HPP4 fragments amplified at 72℃ are identical to the reference sequence (NM_013556.2). The HPP4 fragment amplified at a T_c of 80℃ also shows complete sequence similarity to the reference sequence. Consequently, no sequence changes are apparent, even after mutation enrichment via COLD-PCR. Although the insertion of the amplified *hprt1* fragments into the pEZSeq™ HC Amp Vector introduces a bias towards base changes rather than sequence changes due to insertion or deletions, the results from the dideoxy sequencing correlate with the HRM results. Since HRM was performed directly after PCR, insertions and deletions would have resulted in large T_m changes. The correlation between the HRM and sequencing results therefore indicates that no changes, i.e. basepair changes, strand switching of basepairs, or insertions or deletions, have occurred in the amplified mouse *hprt1* fragments.

These HRM and sequencing results of the mouse *hprt1* fragments correspond with the results of HRM and sequencing of human *fah* and *hprt1* fragments. The results of all of the HRM and sequencing reactions imply the absence of an increased mutation rate, which would have resulted in an increase of mutations. However, only very small fragments of the genomes were investigated. The presence of *de novo* mutations on other parts of the genome can therefore not be excluded. A certain degree of clonal expansion of the mutation would furthermore be required, in order for the mutation to be detectable with the currently available technologies.